I&EC research
Industrial & Engineering Chemistry Research
pubs.acs.org/IECR
Article

DNA Binding by an Intrinsically Disordered Elastin-like Polypeptide for Assembly of Phase Separated Nucleoprotein Coacervates

Telmo Díez Pérez,[#] Adam Quintana,[#] Jacqueline A. De Lora,[#] Andrew P. Shreve, Gabriel P. López, and Nick J. Carroll*

Cite This: *Ind. Eng. Chem. Res.* 2021, 60, 17408−17416

ABSTRACT: The formation of condensed phase nucleoprotein assemblies, such as membraneless organelles (MLOs), that contribute to gene regulation and signaling within the cell is garnering widespread attention. A critical technical challenge is understanding how interactions between intrinsically disordered protein (IDP) and nucleic acid molecular components affect liquid−liquid phase separation (LLPS) into nucleoprotein condensates. To better understand the physics of LLPS that drive the formation of biomolecular condensates (known as coacervates), we investigate a model IDP system using a cationic elastin-like polypeptide (ELP), "E3", that is engineered to phase separate and bind DNA upon coacervate formation. Using mean field Flory−Huggins (FH) theory, we create ternary phase diagrams to quantify DNA component partitioning within discrete protein- and solvent-rich phases across a range of salt and E3 compositions. We suggest a modified FH theory that combines canonical FH interaction parameters with an approximation of the Debye−Hückel theory to predict the strength of E3−DNA interactions and partitioning with a variable salt concentration. Finally, we establish a simple two-step DNA solution separation/purification assay to highlight the potential utility of our system. This model LLPS biopolymer platform represents an important chemical engineering-based contribution to synthetic biology and DNA technologies, with possible implications for origin of life discussions.

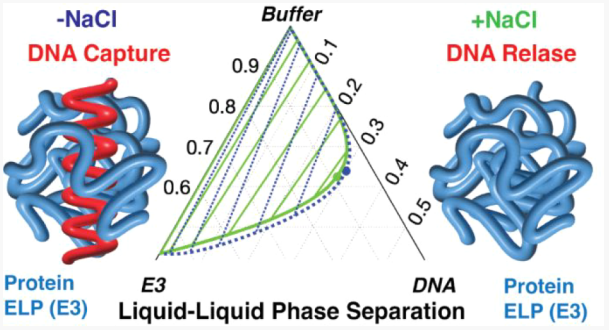

INTRODUCTION

Cellular membraneless organelles (MLOs) are distinct phase separated compartments that lack a lipid membrane but nevertheless function akin to their membrane delineated counterparts via the spatial and temporal organization of molecules. Several MLOs comprise RNA binding intrinsically disordered proteins (IDPs) that undergo reversible liquid−liquid phase separation (LLPS) to assemble and disassemble condensed phase assemblies for a host of regulatory activities. For example, phase separated IDPs bind and sequester cytoplasmic mRNA in MLOs known as stress granules to regulate their activity in response to environmental stresses,[1] sometimes acting with other MLOs such as P-bodies, to regulate mRNA outcome.[2,3] Examples of environmental stimuli that can lead to rapid assembly and disassembly of IDP coacervate MLOs include temperature, pH, and osmotic stress.[4] Cellular MLOs regulate downstream function[5,6] using coupled environmental sensing and molecular phase behavior, thus helping to minimize complex, multilevel signaling cascades.[5,7,8] Hence, condensed phase cellular MLOs provide a practical blueprint to potentially engineer programmable analogs in synthetic systems. Indeed, the simplicity of this biopolymer solution phase behavior is reflected by gaining popularity of IDPs and MLOs in origin of life discussions.[9]

Further inspiring the use of IDPs in engineered systems are investigations that shed light on the mechanism of protein-NA binding[10,11] and the role of IDPs in driving cellular MLO assemblies.[11−13] For example, synthetic nucleoprotein MLOs were assembled in protocells using IDP fusions comprising an elastin-like protein (ELP) block concatenated with a soluble arginine-rich domain (RGG). ELPs are pentameric repeat polymers (sequence VPGXG, X = guest residue),[14,15] while RGG domains are present in a host of cellular IDPs, including LAF-1, FUS, and MRE11.[3,14,15] In that work, the relatively hydrophobic ELP block conferred phase separation behavior to the fusions, while the RGG domain enabled electrostatic binding of the fusions to RNA.[16] In biological systems, RGG domains of cellular IDPs interact with RNA while simultaneously undergoing LLPS and therefore have dual roles as mediators of both RNA-binding phase separation behaviors.[11,17]

Received: July 15, 2021
Revised: November 14, 2021
Accepted: November 14, 2021
Published: November 23, 2021

https://doi.org/10.1021/acs.iecr.1c02823
Ind. Eng. Chem. Res. 2021, 60, 17408−17416

Our understanding of such dual-role IDPs could be bolstered by investigation of synthetic NA-binding IDP surrogates with well-defined stimulus-induced phase behavior that is not driven solely by complexation of IDP and NA polyelectrolytes of opposite charge. In this regard, ELPs are intriguing as candidate surrogates because of their ability to maintain hydrophobic LCST phase behavior even while carrying a relatively large mean net charge.[18] Furthermore, the correlation between the molecular parameters of diverse sets of ELPs (e.g., guest residue, chain length) and their aqueous solubility as a function of temperature, concentration, and presence of cosolutes is well-known. Despite these advantages, interpretation of the relationships between solution component composition as it pertains to ELP phase behavior and on the degree of nucleic acid partitioning within condensed phase ELP coacervates remains a technical challenge.

In this work, we elucidate the phase behavior and DNA binding affinity of a model polycationic ELP (called E3). To produce E3, we engineer an otherwise uncharged ELP to contain equally spaced, interspersed cations that we hypothesize will promote electrostatic binding to DNA after undergoing phase change. E3, with peptide sequence $[(VPGXG)_{10}\text{-}GKG]_8$, comprises 10 subunits of 8 concatenated neutral pentamers (VPGXG, X = 8:2 ratio of Val/Ala), each flanked by cationic Lys residues (see Figure 1A and Table S1 for detailed peptide sequence). It is essential to our investigation that E3 undergoes simple coacervation, driven by a thermodynamic preference for homotypic self-interactions over heterotypic ones, in contrast to charge-mediated complex coacervation, in which oppositely charged polyanions associate to form coacervates in solution. Our results reveal that above a concentration dependent transition temperature (T_T), the model cationic E3 protein undergoes LLPS in the presence or absence of DNA. Furthermore, the condensates formed by simple coacervation can be thermodynamically tuned with NaCl to preferentially interact with single stranded DNA to form synthetic deoxyribonucleoprotein (DNP) coacervates, as depicted schematically in Figure 1B.

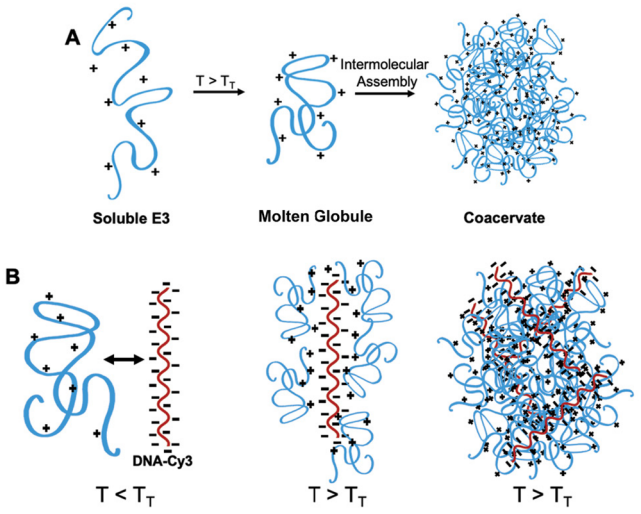

Figure 1. Schematic of E3 coacervate formation and capture of DNA. (A) Illustration of the engineered ELP called "E3" showing the distribution of positively charged Lys residues throughout the random coil protein polymer chain (left). When heated above the transition temperature ($T > T_T$), the E3 chains collapse into molten globule species (middle) that coarsen to form E3-rich coacervates (right). (B) In the presence of negatively charged DNA species, reversible, electrostatically driven interactions between phase transitioned E3 and DNA can occur (left), where condensed E3 molecules bind with DNA (middle), and overtime capture DNA within fully coarsened coacervates (right).

The DNA binding affinity of E3 and the amount of DNA captured and sequestered within E3 coacervates of distinct size and composition are measured systematically at different operating points by varying initial E3 concentration and the addition of charge shielding NaCl salt. We introduce an adapted mean field Flory–Huggins (FH) theory that mediates the strength of E3–DNA interaction by ionic strength through linearization of the Debye–Hückel free-energy in our evaluation of component FH interaction parameters. The FH interaction parameters are fit to fluorescence spectroscopy and microscopy data collected from bulk and from microdroplet samples to create ternary phase diagrams that interpret our experimental observations. Our results showing dependence of FH interaction parameters with ionic strength are corroborated by the Debye–Hückel linearization. This combined approach results in the creation of phase diagrams that quantify DNA component partitioning within discrete protein- and solvent-rich phases of known volume fraction across a range of salt and E3 compositions. Finally, we highlight the utility of our system by prototyping a simple two-step DNA solution purification assay, with implications for applications such as viral RNA extraction, RNA/DNA capture from biological fluids, and gene regulation in synthetic cells

MATERIALS AND METHODS

Expression and Purification of E3. BL21(DE3) *Escherichia coli* cells (One Shot BL21 Star(DE3) Chemically Competent *E. coli*, Thermo Fisher Scientific, Waltham, MA) encoding the E3 gene with kanamycin resistance are incubated on an LB agar plate (Bacto Agar, Becton Dickinson, Franklin Lanes, NJ and Milipore Sigma, St. Louis, MO) with 45 μg/mL kanamycin sulfate (Ultrapure, VWR, Radnor, PA) overnight at 37 °C to grow bacterial colonies for E3 protein expression. Isolated colonies are inoculated into 3 mL of Luria–Bertani Broth (IBI Scientific, Dubuque, Iowa) with 45 μg/mL of kanamycin sulfate. This starter culture is shaken and incubated (Medium Upright GYROMAX 737, Amerex Instruments Inc., Concord, CA) overnight at 220 rpm and 37 °C. The starter culture is then transferred to 1 L of Terrific Broth (IBI Scientific) supplemented with 45 μg/mL of kanamycin for expansion. The culture is incubated and shaken overnight at 37 °C and 220 rpm. The next day, the culture is harvested by centrifugation (Sorvall RC3B Plus, Hyland Scientific, Stanwood, WA) at 4 °C and 3000 rpm for 30 min. To purify the protein, the pellets formed by centrifugation are resuspended with 10–20 mL of lysis buffer containing 50 mL of 1XPBS (phosphate buffered saline, Corning, NY), 1 tablet of protease inhibitor, 50 mL of ethylenediaminetetraacetic acid (0.5 M EDTA, pH 8.0, Invitrogen, Waltham, MA). Then, the resultant cell suspension is sonicated to fully release the lysate or intracellular contents. We then purify the E3 using an inverse transition cycling method developed previously.[19] This method exploits the reversible temperature sensitive phase transition inherent to the protein polymer, allowing it to convert between soluble and insoluble states. Briefly, the approach consists of cyclic centrifugation steps that alternate between hot (38 °C)

https://doi.org/10.1021/acs.iecr.1c02823
Ind. Eng. Chem. Res. 2021, 60, 17408–17416

and cold (4 °C) temperatures in 1× PBS until impurities are removed, typically after 2 to 5 rounds of inverse transition cycling. The product is verified by SDS PAGE (Figure S1).

Measurement of E3 Cloud Point T_T in the Presence of DNA by UV−vis Spectroscopy. Compositions of all DNA species used in the experiments described throughout the remainder of the methods section are given in Table S2. Samples containing a range of E3 concentrations, 500 nM of single stranded 28 nucleotide (nt) DNA (Integrated DNA Technology, Coralville, Iowa), and buffer are prepared according to Table S3. We quantify the transition temperature by measuring the absorbance of the samples at 380 nm, without and with 500 nM ssDNA, as a function of temperature with a temperature controlled (Peltier temperature controller, Agilent, Santa Clara, CA) UV−vis spectrophotometer (Cary 300 UV−vis, Agilent) using previously described methods.[20] The data are then plotted to display the change in absorbance of the solution over a temperature range of 30−60 °C (Figure S2) and the T_T is obtained by taking the maximum in the first derivative of the absorbance as a function of temperature.[20]

Characterization DNA Concentration by Fluorescence Spectroscopy. We design a temperature- and time-dependent fluorescence spectroscopy assay to characterize the binding interactions between E3 and DNA-Cy3 (28 nt single-stranded oligonucleotide with cyanine-3 fluorophore attached to the 5′ end, Table S2) in the presence or absence of 100 mM NaCl (VWR). As depicted in Table S4 and Figure S3, 1 mL of total volume sample solutions in triplicate, at either 0 or 100 mM NaCl, are prepared. The experimental samples consist of E3 at varying concentrations, 500 nM DNA-Cy3, 100 mM sodium phosphate buffer (sodium phosphate powder, Sigma-Aldrich, St Louis, Missouri), and molecular biology-grade water (Corning) at pH 7.0 to maintain E3 phase transition behavior, charge of the Lys residues distributed within the E3 polymers in solution, and a stable pH.[21] All samples are prepared using dark, LightSafe 1.5 mL polypropylene microcentrifuge tubes (Sigma-Aldrich). Control samples, as detailed by asterisks in Table S4, are prepared and treated as experimental samples, to control stability of the fluorescence intensity of Cy3, and used to normalize the measured fluorescence intensity values. The workflow of the measurements is illustrated in Figure S3. The solutions are vortexed and centrifuged for 5 s to combine, then pipetted at room temperature (23 °C) into 100 μL precision volume quartz cuvettes (Ultra-Micro Cell 105.250-QS LP 10 mm × 2 mm, CH 8.5 mm, Hellma Analytics, Plainview, NY). We measure the fluorescence intensity of the samples using a fluorimeter (PTI QuantaMaster QM-400 Horiba, Irvine, CA) with 520 nm excitation wavelength and 540−650 nm emission scan settings (Figures S4 and S5, blue circles). Next, we transfer the sample volumes from the cuvettes back into the dark microcentrifuge tubes to be incubated at 55 °C in a heating block (Isoblock Dry Bath Heat Block, Benchmark, Edison, NJ) for 2 h to induce phase separation of E3 that results in the formation of a clear protein-poor phase and a protein-rich phase settled into the bottom of the tube. By deliberate pipetting, we transfer the supernatant-only (protein-poor phase) to the quartz cuvettes, making sure to leave the coacervate phase undisturbed at the bottom of the tube. We measure the fluorescence intensity of the supernatant by fluorimetry with the same aforementioned settings (Figures S4 and S5, red squares). This enables the determination of the amount of DNA-Cy3 present in the supernatant vs the amount of DNA-Cy3 associated with E3 in the coacervate phase as plotted in Figure 4A. The same procedure is applied to track the location of E3 and DNA in the DNA purification assay depicted in Figure 5A. We design and validate a two-step/two-color isolation assay to quantify the concentration of DNA isolated from a starting mixed sample of E3 and DNA using fluorimetry. Briefly, we measure the fluorescence of E3 doped with E3−Alexa488 (Table S6), with a 450 nm excitation wavelength and 470−540 nm emission scan settings, along with 500 nM DNA-Cy3 at room temperature (Figure 5A and Figure S9). Next, we incubate the solutions at 55 °C to induce E3 phase separation. Two phases form and we decant the supernatant of the solution and resuspend the coacervate with 500 mM NaCl to measure by fluorimetry, allowing us to track the location of the green emission from E3−488 vs the red emission from DNA-Cy3.

Fluorescence Microscopy Imaging. To image the process of temperature-mediated E3 coacervation and interaction with DNA-Cy3, we use an Olympus IX83 fluorescence microscope (Olympus Life Science Technology Division, Center Valley, PA) equipped with a Physitemp cooling and heating stage (TS4-MP/ER/PTU, Clifton, NJ) fitted with a temperature controller. Microfluidic droplets are generated using previously described methods with the droplet generator shown in Figure S6. These droplets contain different E3 concentrations, 500 nM DNA-Cy3, sodium phosphate buffer at pH 7.0, and either 0 or 100 nM added NaCl (Table S5, Figure S6), and are pipetted onto a glass slide (18 mm × 18 mm Square Micro Cover Glass, VWR). The droplet population is allowed to settle for 5 min until there is a single layer of droplets on the surface. The glass slide is mounted onto the temperature-controlled stage and equilibrated to 20 °C. Images are acquired by a high dynamic range camera (ORCA-Flash4.0 V3 Digital CMOS camera C13440-20CU, Hamamatsu, Bridgewater, NJ) using both brightfield and fluorescence (520 nm LED excitation source/550 nm emission filter) acquisition modes, across a temperature range including values below (25 °C), and above the T_T (55 °C) (Figure 3) until complete LLPS is achieved.

Ternary Component Flory−Huggins Phase Diagrams. The standard FH equation providing the Helmholtz free energy density f for an incompressible two-polymer aqueous system of polymer volume fraction components ϕ_1 and ϕ_2 is[22,23]

$$f = \frac{\phi_1 \ln \phi_1}{N_1} + \frac{\phi_2 \ln \phi_2}{N_2} + \phi_s \ln \phi_s + \chi_1 \phi_1 \phi_s + \chi_2 \phi_2 \phi_s + \chi_x \phi_1 \phi_2 \quad (1)$$

where χ_i are pairwise interaction parameters with the solvent and χ_x is the interaction parameter for components 1 and 2. The degree of polymerization N_1 and N_2 are the ratios, with respect to solvent, of the molar volumes of E3 and DNA, respectively. The solvent volume fraction ϕ_s is given by the volume fraction conserving condition $1 = \sum_i \phi_i$. The criteria for phase equilibria in a multicomponent system is the equality of chemical potential (given as $\mu_i = \frac{\partial f}{\partial \phi_i}$) between all phases for each component. With the volume fraction conservation constraint, the buffer chemical potential is no longer independent of the other components.[24] In its place analytically is the constraint of equivalent excess grand free-energy between phases, which is otherwise known as a Weierstrass-Erdmann condition.[25] These criteria are summarized as

https://doi.org/10.1021/acs.iecr.1c02823
Ind. Eng. Chem. Res. 2021, 60, 17408−17416

$$\mu_1(\phi_1', \phi_2') = \mu_1(\phi_1'', \phi_2'') = \mu_1^* \quad (2)$$

$$\mu_2(\phi_1', \phi_2') = \mu_2(\phi_1'', \phi_2'') = \mu_2^* \quad (3)$$

$$f(\phi_1', \phi_2') - f(\phi_1'', \phi_2'') = (\phi_1' - \phi_1'')\mu_1^* + (\phi_2' - \phi_2'')\mu_2^* \quad (4)$$

Here ϕ_i' and ϕ_i'' denote the volume fraction of component i in the dilute and dense phases, respectively. There exists one set of the binodal chemical potentials $\{\mu_1^*, \mu_2^*\}$ for each tie line within the phase envelope, given explicitly as the set $\{\phi_1', \phi_1'', \phi_2', \phi_2''\}$. Therefore, the coupled set of equations can be determined experimentally by determining $\{\phi_1', \phi_1'', \phi_2', \phi_2''\}$ for a unique set of FH parameters.

RESULTS AND DISCUSSION

ssDNA Influences the Phase Behavior of Aqueous E3. To quantify the effect of ssDNA (0.5 μM, 28 nt) on the thermally dependent phase behavior of E3 (sequence: $[(VPGXG)_{10}\text{-}GKG]_8$, X = 8:2 ratio of Val/Ala), we use temperature-controlled spectrophotometry to measure cloud-point transition temperature (T_T) as a function of volume fraction (ϕ)—the fraction of solution volume occupied by E3 chains—for E3 in the presence or absence of ssDNA species (+ssDNA or −ssDNA, respectively). We measure E3 $T_T(\phi)$ for volume fractions ranging from ϕ = 0.00034 to ϕ = 0.068 in pH-stable buffer (Table S3 and Figure S2). The range of ϕ values corresponds to E3 concentrations of 0.01 mM to 2 mM. The E3 polymer maintains canonical ELP LCST dilute phase behavior[26,27]—a decrease in T_T with increasing E3 volume ϕ—for both + ssDNA and −ssDNA solutions. We find, however, for all replicate samples that the presence of ssDNA prompts a shift to lower $T_T(\phi)$ (Figure 2, red squares) across

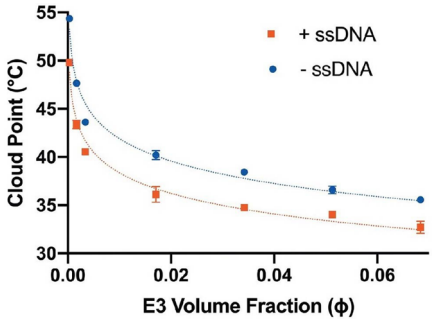

Figure 2. Characterization of E3 $T_T(\phi)$ in the absence and presence of 0.5 μM ssDNA. Average T_T with standard deviations as a function of E3 volume fraction (ϕ) in the presence (red squares) and absence (blue circles) of DNA (0.5 μM, 28 nt) are plotted. The dashed lines represent the best logarithmic fit for ELP (E3) at + and −ssDNA conditions.

all experimental ϕ values when compared to $T_T(\phi)$ for the −ssDNA E3 replicate samples (Figure 2, blue circles). These results motivate further investigation to understand how DNA alters the phase behavior of E3 in aqueous buffer and how the partitioning of DNA with E3 condensates can be modulated.

NaCl Mediates Recruitment of ssDNA into E3 Condensates. We investigate the temperature- and salt-mediated partitioning of ssDNA with phase transitioned E3 condensates. Microfluidic generated water-in-oil emulsions provide us with a useful window into the microenvironment to better understand LLPS as it relates to E3−ssDNA binding behavior. We trigger ELP phase transition within microdroplets by increasing the temperature (T = 55 °C) above the T_T of 1 mM E3 (ϕ = 0.034, $T_{T+ssDNA}$ = 35 °C) to generate coarsening spherical E3 condensates surrounded by solvent-rich regions. Observing the evolution of the thermally phase transitioned system from 0 to 15 min, we track the coarsening of unlabeled E3 to completion and the concurrent partitioning of fluorophore labeled ssDNA-Cy3 in each phase by brightfield and fluorescence microscopy, respectively. The interaction between droplet encapsulated components of 1 mM E3 (brightfield), 0.5 μM ssDNA-Cy3 (fluorescence), and the influence of 0 or 100 mM NaCl salt (−NaCl and +NaCl, respectively) in aqueous droplets is detailed. For both − and + NaCl samples, we show representative droplet microscopy images at (1) t = 0 min at room temperature, $T < T_T$, where E3 is in a soluble state; (2) t = 3 min of incubation at $T > T_T$ during the early stages of phase separation and E3 condensate coarsening; and (3) t = 15 min at $T > T_T$ when full coarsening and complete phase separation is achieved.

Across all t = 0 samples at room temperature ($T < T_T$) no E3 condensates are observed (Figure 3, A1 and D1) and all solution components are miscible and evenly distributed throughout the droplet volume (Figure 3A2,D2,A3,D3). The incipient stages of thermally triggered E3 phase transition occur simultaneously throughout droplet volumes, corroborating demixing through spinodal decomposition for both + NaCl and − NaCl samples (Figure 3, B1 and E1). After coarsening completes, each microdroplet exhibits a monodisperse core−shell arrangement in which the spherical core is an E3-rich condensate, and the surrounding shell is an aqueous-rich phase (Figure 3, C1 and F1). Time lapse fluorescence microscopy of ssDNA-Cy3 reveals that above T_T and without added NaCl, the fluorescent ssDNA-Cy3 is efficiently captured and localized within E3 condensates—noticeable even during the early stages of spinodal decomposition (Figure 3E2,E3 and Supplemental movie). Note that the recruitment of ssDNA-Cy3 into the E3 rich condensates is E3 concentration dependent (Figure S7). By contrast, the addition of NaCl results in electrostatic shielding,[28,29] partitioning much more ssDNA-Cy3 in the solvent-rich phase (Figure 3, B2 and C2). The combined E3 phase behavior and ssDNA-Cy3 partitioning for −NaCl and +NaCl is further evidenced by inspection of the merged brightfield and fluorescence microscopy images of Figure 3, panels A3−F3.

Flory−Huggins Phase Diagrams Describe NaCl Mediated DNA Capture by E3 Condensates. Using FH formalisms (see eqs 1−4), we approximate the phase diagrams of solution E3 and DNA and at two salt concentrations of 0 mM NaCl and 100 mM NaCl. To quantify the partitioning of DNA into E3 coacervates at 0 mM and 100 mM NaCl, we use fluorimetry to determine DNA concentration in the dilute solvent-rich phase (Figure 4A, Figures S4 and S5) and microscopy to determine the total volume fraction occupied by E3 coacervates as measured in microdroplets (Figure 4B), for a range of E3 concentrations (T = 55 °C). Hence, the experimentally available data for fitting the FH parameters $\chi = \{\chi_{E3,Buffer}, \chi_{DNA,Buffer}, \chi_{E3,DNA}\}$ are the concentration variant supernatant DNA concentration ratio from initial $\left(\frac{C'}{C_0}\right)_{DNA}$ and the total volume fraction of the E3 coacervate

https://doi.org/10.1021/acs.iecr.1c02823
Ind. Eng. Chem. Res. 2021, 60, 17408−17416

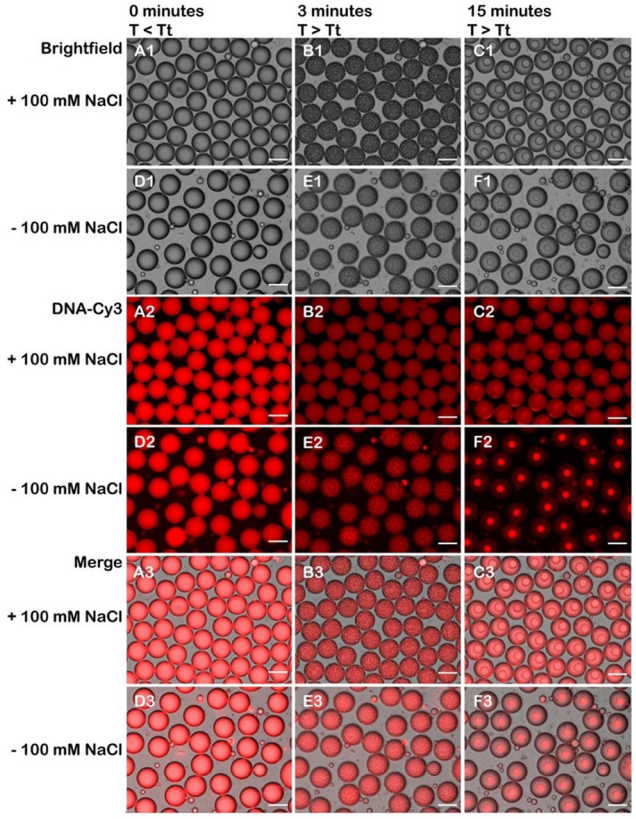

Figure 3. Phase and ssDNA-Cy3 partitioning behavior of 1 mM E3 within aqueous microdrops in oil: with added NaCl (+100 mM NaCl) and with no added NaCl (−100 mM NaCl). (A1−F1) Brightfield microscopy shows thermally induced spinodal decomposition of E3 (1 mM initial concentration) into fully coarsened condensate spheres, with similar phase behavior for both +and −NaCl solutions. (A2−F2) Time lapse fluorescence microscopy of ssDNA-Cy3 (0.5 μM, red). Above the E3 T_T (T = 55 °C) and without added NaCl, the fluorescent DNA is efficiently sequestered in E3 condensates. Adding NaCl results in electrostatic shielding leaving much more of DNA in the solvent-rich phase. (A3−F3) Overlay of time lapse brightfield and fluorescence microscopy images depicting E3 phase separation and concurrent ssDNA-Cy3 localization in microdrops at T = 55 °C. Scale bars = 50 μm.

$$p = \frac{\phi_{E3} - \phi'_{E3}}{\phi''_{E3} - \phi'_{E3}} = \frac{\phi_{DNA} - \phi'_{DNA}}{\phi''_{DNA} - \phi'_{DNA}}$$

In FH theory, component i volume fraction is related to concentration by the molar volume of the buffer (ν) by $\phi_i = \frac{\nu N_i C_i}{1 + \nu \sum_i N_i C_i}$.[30]

Without independent phase data of DNA in buffer, the DNA−buffer interaction parameter $\chi_{DNA,\ Buffer}$ is unknown. We found that keeping the difference $\chi_{DNA,\ Buffer} - \chi_{E3,\ DNA}$ constant while varying $\chi_{E3,\ DNA}$ appears to generate nearly equivalent dilute-phase DNA volume fractions. Therefore, keeping $\chi_{DNA,\ Buffer} = 0$ while finding the best fitting $\chi_{E3,\ DNA}$ will generate the best set of χ knowing that only $\chi_{DNA,\ Buffer} - \chi_{E3,\ DNA}$ is expected to be unique. The solution E3 interaction parameter at T = 55 °C was reported in our previous work[20] ($\chi_{E3,\ Buffer}$ = 0.862) and is assumed to be constant for both salt conditions. For approximation, we assume the degree of polymerization of the E3 is equal to the number of pentameric repeats of the protein (i.e., VPGXG), in this case N_{E3} = 80. For the DNA degree of polymerization, we shall assume that molar volume ratio is equal to molecular weight ratio between molecules, giving $N_{DNA} = \frac{M_{DNA}}{M_{E3}} N_{E3} \approx 20$.

Fitting FH eqs 1−4 to the dilute phase DNA concentration ratio data simultaneously with the coacervate volume fraction data enables determination of the cross-polymer interaction parameter $\chi_{E3,\ DNA}$ and the buffer molar volume ν at 0 mM NaCl and 100 mM NaCl conditions (see Figure S8 for multivariate fits). Specifically, phase diagram tie line interpolation was used to find the best fitting buffer molar volume for a variance of $\chi_{E3,\ DNA}$ for both measurements. Then, the intersection of the best fitting lines from each measurement determined the overall best fit. We find that 0 mM NaCl results in the interaction parameter $X_{E3,\ DNA}$ = −1.0 and the 100 mM NaCl resulted in a larger $X_{E3,\ DNA}$ = −0.54. The interpolation of the tie lines from the resulting phase diagrams of the experimental concentrations used are presented in Figure 4A showing the depression of DNA in the supernatant phase for the 0 mM NaCl condition, corresponding to enhanced DNA partitioning in the E3 coacervate, and the constant ratio of DNA for the 100 mM NaCl condition. These results are in agreement with observations described in Figure 3.

The best fitting buffer molar volume ν was found to be 0.54 M^{-1} and 0.58 M^{-1} for the − and + NaCl, respectively, and a mean value of 0.56 M^{-1} was used for analysis. With respect to the experimental variance of the microdroplet measurements of Figure 4B, a small change from the addition of 100 mM NaCl suggests a nominal effect of excluded volume from increasing ionic concentration of a buffer solution, which is corroborated from the literature.[31] Furthermore, the value for buffer molar volume should be recognized as being referenced by the assumed chain length. As the chain length of E3 was assumed to be the number of pentameric repeats, N_{E3} = 80, this molar volume suggests that each VPGXG unit will occupy 560 cm^3/mol or 112 cm^3/mol for each amino acid.

We suggest an appendage to FH that could be used to describe the change in interaction parameters leading to partitioning of DNA with E3 coacervates at various NaCl concentrations. We assume the ionic effects are captured on a mean field level by introducing an enthalpic free energy provided by the Debye−Hückel (DH) theory. Considering the solvation criteria for DH, it should be admissible to assume the ionic effects contribute by appending the standard FH interaction parameters with a linear perturbation for charge effects. Each effective interaction parameter $\chi_{i,j}$ will be, by a first approximation, the hypothetical interaction parameter of the same system without Coulombic interactions $\chi^0_{i,j}$ appended with the respective term from a linearization of the DH free energy (see Supporting Information, eqs 1−15 for derivation of linear DH terms).

$$\chi_{E3,Buffer} = \chi^0_{E3,Buffer} + 2A\frac{\sqrt{I_s}}{1 + \sqrt{I_s}}(I_s - \alpha_{E3}) \quad (5)$$

$$\chi_{DNA,Buffer} = \chi^0_{DNA,Buffer} + 2A\frac{\sqrt{I_s}}{1 + \sqrt{I_s}}(I_s - \alpha_{DNA}) \quad (6)$$

https://doi.org/10.1021/acs.iecr.1c02823
Ind. Eng. Chem. Res. 2021, 60, 17408−17416

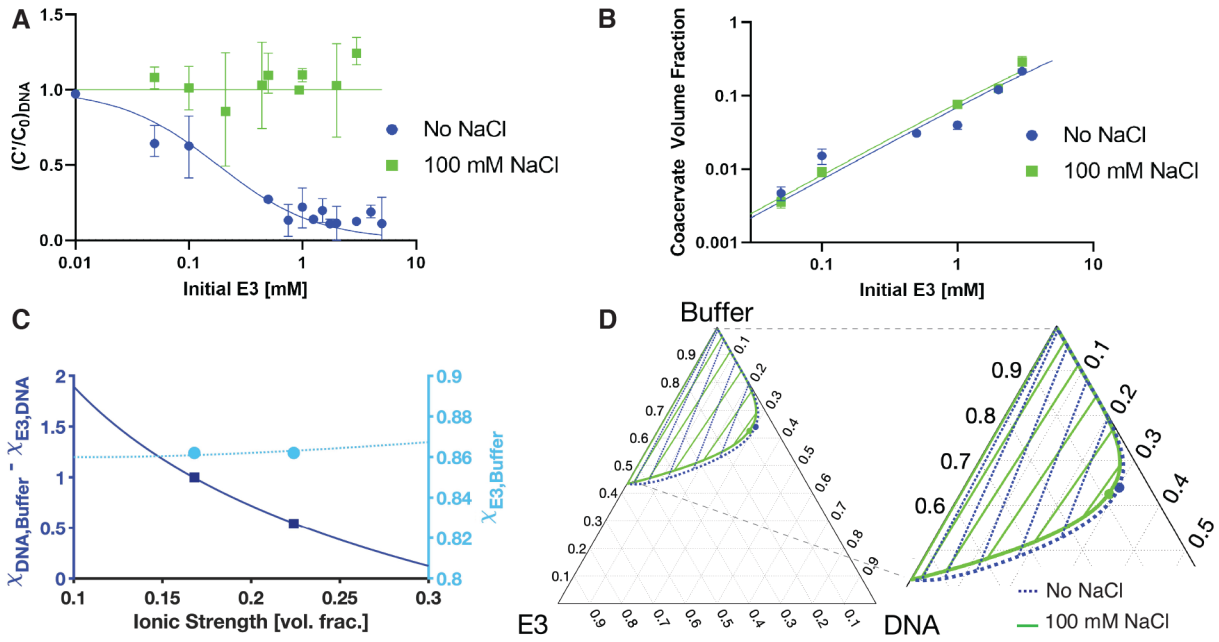

Figure 4. Salt-mediated DNA capture by E3 coacervates at T = 55 °C. Experimental data (marker points with standard deviation) of (A) dilute phase DNA concentration fraction from initial $(C'/C_0)_{DNA}$ and (B) E3 coacervate volume fraction in microdrops used as FH fitting parameters (solid curves are interpolations of the tie lines from resulting FH phase diagrams). (C) Dependence on ionic strength for Debye−Hückel modified FH interaction parameters (lines) and experimental FH interaction parameters (marker points). (D) Ternary phase diagrams comprising binodal curves and a few representative tie lines for E3, DNA, and buffer for added salt concentrations of 0 mM NaCl (green, solid lines) and 100 mM NaCl (blue, dashed lines). Critical points are marked as circles.

$$\chi_{E3,DNA} = \chi^0_{E3,DNA} - A\left(\frac{(\alpha_{E3} - I_s)(\alpha_{DNA} - I_s)}{\sqrt{I_s}(1+\sqrt{I_s})^2} + \frac{2\sqrt{I_s}}{1+\sqrt{I_s}}(2I_s - \alpha_{E3} - \alpha_{DNA})\right) \quad (7)$$

Here, A is the Debye−Huckel free-energy prefactor which is related to ionic radius.[24] I_s is the ionic strength of the salt solution multiplied with the buffer molar volume ν. The I_s value for our 100 mM dibasic sodium phosphate buffer at 0 and 100 mM added NaCl is 0.3 M and 0.4 M, respectively. The component of ionic strength for each polyion is given as $\alpha_i = \frac{z_i^2}{2N_i}$, where z_i is the total number of charges of molecule i.

Figure 4C shows the dependence on NaCl of DH modified FH interaction parameters and agrees with the experimentally determined interaction parameters. The other fitted parameters are the DH free energy prefactor A = 0.1 and the non-Columbic interaction parameters $\chi^0_{E3,Bufffer}$ = 0.874 and $\chi^0_{DNA,Bufffer} - \chi^0_{E3,DNA}$ = 2.71. The small variance for $\chi_{E3,Buffer}$ is the likely result of a small ionic strength component of E3 (α_{E3} = 0.4) as the change from − to + NaCl leads to a total change $\Delta\chi_{E3,Buffer}$ = 0.002. This contrasts with the larger change from the DNA−buffer interaction parameter with α_{DNA} = 19.6 and $\Delta\chi_{DNA,Buffer}$ = −0.12. However, these differences are expected to be strongly dependent on the choice for polymer chain length, as this value will directly affect the resulting buffer molar volume.

Fully determining the FH parameters N and χ allows for the determination of the full three component phase diagram, including the binodal, tie lines, and critical point, and these plots are given in Figure 4D. It should be noted that the underlying interaction parameters were determined in a dilute DNA limit and the extrapolation to higher concentration has not been validated. Nonetheless, these plots show the fundamental contrast that increasing salt concentration has on DNA phase partitioning with E3. Namely, increasing salt concentration will lower the equilibrium concentration of DNA in the E3 coacervate. This behavior is illustrated by dissimilar tie line slopes for − and + NaCl, where intersections with the binodal gives the equilibrium component volume fraction in each phase. Furthermore, this observation is corroborated by Debye−Hückel theory.

Sequential LLPS Allows Recovery of DNA from E3/DNA Solutions. The fact that E3 efficiently captures DNA upon coacervation only in the absence of added salt suggests a potential simple means for separation of DNA from solutions by LLPS. As depicted in Figure 5, we design and validate a two-step/two-color assay to quantify the concentration of DNA isolated from a starting mixed sample of E3 and DNA using fluorimetry. Briefly, we measure the fluorescence of 0.5 mM E3 doped with E3-labeled by Alexa 488 (E3−488, see Table S6) along with 500 nM DNA-Cy3 at room temperature (Figure 5A and Figure S9 yellow circles, baseline and control, to represent 100% fluorescence intensity). Next, we incubate the solutions at 55 °C to induce E3/DNA phase separation. As previously observed in Figure 3, the DNA localizes to the protein-rich (coacervate) phase upon this first LLPS process. We then discard the supernatant and resuspend the coacervate with 500 mM NaCl (Step 1 in Figure 5) and measure fluorescence intensities (Figure 5B, left bars; Figure S9, blue squares); over 80% of E3 and DNA are retained through this process. Next, in Step 2, we incubate the resuspended coacervate at 55 °C to induce phase transition of E3 in the presence of 500 mM NaCl. After this second round of LLPS, we measure the fluorescence of the supernatant and find the

https://doi.org/10.1021/acs.iecr.1c02823
Ind. Eng. Chem. Res. 2021, 60, 17408−17416

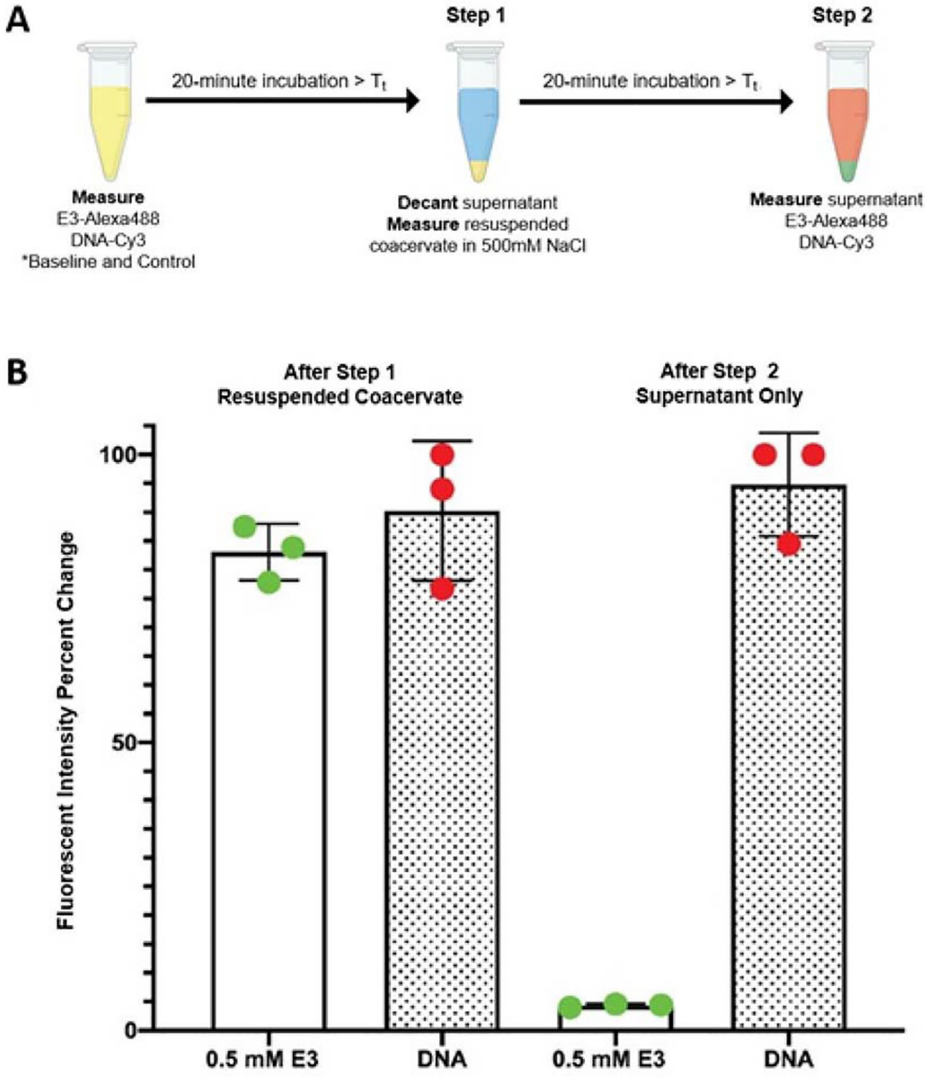

Figure 5. Two-step DNA purification assay. (A) Workflow for the two-step DNA isolation assay. (B) Results of fluorimetry measurements taken after step 1 (left side) and after step 2 (right side). E3−488, green circles/blank bars; DNA-Cy3, red circles/spotted bars. Each circle represents a measurement of the individual sample; the bars show the average of the circular data points and the error bars show the standard deviation.

DNA-Cy3 intensity to be comparable to the original DNA-Cy3 measured before the first incubation. Meanwhile, the signal of E3−488 decreases by 95% under these conditions, demonstrating an efficient separation and recovery of DNA from protein solution upon the addition of salt (Figure 5B, right bars; Figure S9, red triangles). These results are in agreement with findings detailed in Figures 3 and 4. Figure 4A and Figure S4 suggest that the initial (i.e., prior to LLPS) ELP concentration should be equal to, or in excess of, 0.5 mM for efficient capture of 500 nM DNA within the coacervate phase under low salt conditions. These results suggest that triggered LLPS of NA-binding IDPs may be an efficient means of isolating nucleic acids from complex solutions that avoid the use of expensive consumables such as spin columns or magnetic beads.[32,33] We investigate this prospect in detail in a forthcoming study.

■ CONCLUSION

In this work, the phase behavior and molecular partitioning of a ternary component ELP, DNA, and aqueous buffer solution system are investigated. We engineer a model ELP called E3 that comprises ELP blocks flanked by eight evenly spaced, cationic lysine residues (E3 sequence: $[(VPGXG)_{10}\text{-}GKG]_8$, X = 8:2 ratio of Val:Ala). The concentration-dependent LCST transition temperature of E3 is reduced by a few degrees Celsius in the presence of DNA. The NaCl-mediated capture of fluorescently labeled Cy3 DNA by E3 condensates is observed in microfluidic generated drops and characterized by fluorescence spectroscopy. Our results show E3 efficiently captures DNA upon coacervation only in the absence of added NaCl salt, and at 100 mM added NaCl, DNA shows no preference for the coacervate or solvent-rich phase. Mean field Flory−Huggins (FH) theory describes the drastic reduction in DNA partitioning by E3 coacervates with the addition of 100 mM NaCl. We use a multivariate fitting of FH interaction parameters to experimental data of a concentration-variant supernatant DNA concentration ratio from the initial and the total volume fraction of E3 coacervates. We introduce the addition of a linearized Debye−Hückel term to FH interaction parameters to account for variable E3 condensate DNA capture as a result of change in ionic strength. Our results show similar changes in the DH-modified FH interaction parameters

https://doi.org/10.1021/acs.iecr.1c02823
Ind. Eng. Chem. Res. 2021, 60, 17408−17416

as those estimated from fitting to experimental data. We generate ternary phase diagrams complete with tie lines and binodal curves that quantify DNA and E3 component partitioning within protein- and solvent-rich phases at 0 mM and 100 mM added NaCl buffer conditions. Finally, we demonstrate the utility of our system by prototyping a new DNA purification assay by using thermal LLPS of E3 and the addition of NaCl salt to control the DNA binding and release behavior of E3 condensates.

■ ASSOCIATED CONTENT

Supporting Information

. The Supporting Information is available free of charge at https://pubs.acs.org/doi/10.1021/acs.iecr.1c02823.

Amino acid, nucleic acid composition, protein gel, experimental compositions, micrographs, device schematic, absorbance and fluorescence spectroscopy measurements, and D.H. equations (PDF)

Thermally induced E3 phase separation and DNA capture in microdrops (AVI)

■ AUTHOR INFORMATION

Corresponding Author

Nick J. Carroll − *Center for Micro-Engineered Materials and Department of Chemical and Biological Engineering, University of New Mexico, Albuquerque, New Mexico 87131, United States;* orcid.org/0000-0001-7747-7307; Email: ncarroll@unm.edu

Authors

Telmo Díez Pérez − *Center for Biomedical Engineering, Center for Micro-Engineered Materials, and Department of Chemical and Biological Engineering, University of New Mexico, Albuquerque, New Mexico 87131, United States*

Adam Quintana − *Department of Chemical and Biological Engineering, University of New Mexico, Albuquerque, New Mexico 87131, United States*

Jacqueline A. De Lora − *Center for Biomedical Engineering and Department of Chemical and Biological Engineering, University of New Mexico, Albuquerque, New Mexico 87131, United States; Max Planck Institute for Medical Research, Department of Cellular Biophysics, Heidelberg 69120, Germany;* orcid.org/0000-0001-5599-7838

Andrew P. Shreve − *Center for Biomedical Engineering and Department of Chemical and Biological Engineering, University of New Mexico, Albuquerque, New Mexico 87131, United States;* orcid.org/0000-0002-9567-3181

Gabriel P. López − *Center for Biomedical Engineering and Department of Chemical and Biological Engineering, University of New Mexico, Albuquerque, New Mexico 87131, United States;* orcid.org/0000-0002-5383-0708

Complete contact information is available at: https://pubs.acs.org/10.1021/acs.iecr.1c02823

Author Contributions

All the authors contributed to the writing of this paper. T.D.P. expressed and purified ELP proteins used in the experiments, performed UV−vis spectroscopy experiments, and constructed droplet microfluidic devices. A.Q. conducted theoretical analysis that includes envisaging of the modified FH theory, MATLAB coding, and parametric analysis to generate ternary phase diagrams. J.A.D. prepared samples, performed fluorimetry experiments and graphic design of figures. A.P.S. assisted with planning, execution, and interpretation of fluorimetry experiments. G.P.L. contributed expertise and training in experimental design, recombinant biomaterials, and theoretical analysis. N.J.C. directed all experiments, measurements and theory, provided intellectual guidance, and approved final edits to the manuscript.

Author Contributions

#T.D.P., A.Q., and J.A.D. contributed equally to this paper.

Notes

The authors declare no competing financial interest.

■ ACKNOWLEDGMENTS

This invited contribution is part of the I&EC Research special issue for the 2021 Class of Influential Researchers. We kindly thank Andrew Owens for assistance in protein and microfluidics experiments and Qing Sun for assistance with protein synthesis. G.P.L, T.D.P., and N.J.C. received funding from National Science Foundation EAGER [CBET-2031774]. T.D.P. and N.J.C. received funding from National Science Foundation EAGER [CBET-1843958]. N.J.C. and A.Q. received funding from National Science Foundation CAREER [CBET-2048051]. N.J.C. and J.A.D. received funding for materials from The University of New Mexico Chemical and Biological Engineering Department; A.Q. received funding from National Science Foundation Graduate Research Fellowship Program [DE-1939267]. J.A.D. received funding from the Max Planck Society.

■ REFERENCES

(1) Protter, D. S. W.; Parker, R. Principles and Properties of Stress Granules. *Trends Cell Biol.* **2016**, *26* (9), 668−679.

(2) Kulkarni, M.; Ozgur, S.; Stoecklin, G. On track with P-bodies. *Biochem. Soc. Trans.* **2010**, *38*, 242−51.

(3) Elbaum-Garfinkle, S.; Kim, Y.; Szczepaniak, K.; Chen, C. C. H.; Eckmann, C. R.; Myong, S.; Brangwynne, C. P. The disordered P granule protein LAF-1 drives phase separation into droplets with tunable viscosity and dynamics. *Proc. Natl. Acad. Sci. U. S. A.* **2015**, *112* (23), 7189−7194.

(4) Marnik, E. A.; Updike, D. L. Membraneless organelles: P granules in Caenorhabditis elegans. *Traffic* **2019**, *20* (6), 373−379.

(5) Anderson, P.; Kedersha, N. RNA granules. *J. Cell Biol.* **2006**, *172* (6), 803−808.

(6) Calabretta, S.; Richard, S. Emerging Roles of Disordered Sequences in RNA-Binding Proteins. *Trends Biochem. Sci.* **2015**, *40* (11), 662−672.

(7) Brangwynne, C. P. Soft active aggregates: mechanics, dynamics and self-assembly of liquid-like intracellular protein bodies. *Soft Matter* **2011**, *7* (7), 3052−3059.

(8) Hyman, A. A.; Brangwynne, C. P. Beyond Stereospecificity: Liquids and Mesoscale Organization of Cytoplasm. *Dev. Cell* **2011**, *21* (1), 14−16.

(9) Luisi, P. L. *The emergence of life: from chemical origins to synthetic biology*; Cambridge University Press: Cambridge, 2016.

(10) Ozdilek, B. A.; Thompson, V. F.; Ahmed, N. S.; White, C. I.; Batey, R. T.; Schwartz, J. C. Intrinsically disordered RGG/RG domains mediate degenerate specificity in RNA binding. *Nucleic Acids Res.* **2017**, *45* (13), 7984−7996.

(11) Schuster, B. S.; Reed, E. H.; Parthasarathy, R.; Jahnke, C. N.; Caldwell, R. M.; Bermudez, J. G.; Ramage, H.; Good, M. C.; Hammer, D. A. Controllable protein phase separation and modular recruitment to form responsive membraneless organelles. *Nat. Commun.* **2018**, *9*, 2985.

(12) Protter, D. S. W.; Rao, B. S.; Van Treeck, B.; Lin, Y.; Mizoue, L.; Rosen, M. K.; Parker, R. Intrinsically Disordered Regions Can

Contribute Promiscuous Interactions to RNP Granule Assembly. *Cell Rep.* **2018**, *22* (6), 1401−1412.
(13) Nott, T. J.; Petsalaki, E.; Farber, P.; Jervis, D.; Fussner, E.; Plochowietz, A.; Craggs, T. D.; Bazett-Jones, D. P.; Pawson, T.; Forman-Kay, J. D.; Baldwin, A. J. Phase Transition of a Disordered Nuage Protein Generates Environmentally Responsive Membraneless Organelles. *Mol. Cell* **2015**, *57* (5), 936−947.
(14) Thandapani, P.; O'Connor, T. R.; Bailey, T. L.; Richard, S. Defining the RGG/RG motif. *Mol. Cell* **2013**, *50* (5), 613−623.
(15) Dery, U.; Coulombe, Y.; Rodrigue, A.; Stasiak, A.; Richard, S.; Masson, J. Y. A glycine-arginine domain in control of the human MRE11 DNA repair protein. *Mol. Cell. Biol.* **2008**, *28* (9), 3058−3069.
(16) Simon, J. R.; Eghtesadi, S. A.; Dzuricky, M.; You, L. C.; Chilkoti, A. Engineered Ribonucleoprotein Granules Inhibit Translation in Protocells. *Mol. Cell* **2019**, *75*, 66.
(17) Wei, M. T.; Elbaum-Garfinkle, S.; Holehouse, A. S.; Chen, C. C. H.; Feric, M.; Arnold, C. B.; Priestley, R. D.; Pappu, R. V.; Brangwynne, C. P. Phase behaviour of disordered proteins underlying low density and high permeability of liquid organelles. *Nat. Chem.* **2017**, *9* (11), 1118−1125.
(18) Quiroz, F. G.; Chilkoti, A. Sequence heuristics to encode phase behaviour in intrinsically disordered protein polymers. *Nat. Mater.* **2015**, *14* (11), 1164−1171.
(19) MacEwan, S. R.; Hassouneh, W.; Chilkoti, A. Non-chromatographic Purification of Recombinant Elastin-like Polypeptides and their Fusions with Peptides and Proteins from Escherichia coli. *J. Visualized Exp.* **2014**, *88*, e51583.
(20) Simon, J. R.; Carroll, N. J.; Rubinstein, M.; Chilkoti, A.; Lopez, G. P. Programming molecular self-assembly of intrinsically disordered proteins containing sequences of low complexity. *Nat. Chem.* **2017**, *9* (6), 509−515.
(21) MacKay, J. A.; Callahan, D. J.; FitzGerald, K. N.; Chilkoti, A. Quantitative model of the phase behavior of recombinant pH-responsive elastin-like polypeptides. *Biomacromolecules* **2010**, *11* (11), 2873−2879.
(22) Iqbal, M.; Tao, Y.; Xie, S.; Zhu, Y.; Chen, D.; Wang, X.; Huang, L.; Peng, D.; Sattar, A.; Shabbir, M. A. B.; Hussain, H. I.; Ahmed, S.; Yuan, Z. Aqueous two-phase system (ATPS): an overview and advances in its applications. *Biol. Proced. Online* **2016**, *18*, 1−18.
(23) Yu, M.; Nishiumi, H.; de Swaan Arons, J. Thermodynamics of phase separation in aqueous solutions of polymers. *Fluid Phase Equilib.* **1993**, *83*, 357−364.
(24) Fisher, M. E.; Levin, Y. Criticality in ionic fluids: Debye-Hückel theory, Bjerrum, and beyond. *Phys. Rev. Lett.* **1993**, *71* (23), 3826.
(25) Eyre, D. J. Systems of cahn−hilliard equations. *SIAM J. Appl. Math.* **1993**, *53* (6), 1686−1712.
(26) Urry, D. W. Physical chemistry of biological free energy transduction as demonstrated by elastic protein-based polymers. *J. Phys. Chem. B* **1997**, *101* (51), 11007−11028.
(27) McDaniel, J. R.; Radford, D. C.; Chilkoti, A. A unified model for de novo design of elastin-like polypeptides with tunable inverse transition temperatures. *Biomacromolecules* **2013**, *14* (8), 2866−2872.
(28) Record, M. T.; Anderson, C. F.; Lohman, T. M. Thermodynamic analysis of ion effects on the binding and conformational equilibria of proteins and nucleic acids: the roles of ion association or release, screening, and ion effects on water activity. *Q. Rev. Biophys.* **1978**, *11* (2), 103−178.
(29) Privalov, P. L.; Dragan, A. I.; Crane-Robinson, C. Interpreting protein/DNA interactions: distinguishing specific from non-specific and electrostatic from non-electrostatic components. *Nucleic Acids Res.* **2011**, *39* (7), 2483−2491.
(30) Flory, P. *Principles of Polymer Chemistry*; Cornell University Press: Ithaca New York, 1953.
(31) Gnutt, D.; Gao, M.; Brylski, O.; Heyden, M.; Ebbinghaus, S. Excluded-volume effects in living cells. *Angew. Chem., Int. Ed.* **2015**, *54* (8), 2548−2551.
(32) Berensmeier, S. Magnetic particles for the separation and purification of nucleic acids. *Appl. Microbiol. Biotechnol.* **2006**, *73* (3), 495−504.
(33) Chomczynski, P.; Sacchi, N. The single-step method of RNA isolation by acid guanidinium thiocyanate−phenol−chloroform extraction: twenty-something years on. *Nat. Protoc.* **2006**, *1* (2), 581−585.

https://doi.org/10.1021/acs.iecr.1c02823
Ind. Eng. Chem. Res. 2021, 60, 17408−17416